Compression After Multiple Low Velocity Impacts of NCF, 2D and 3D Woven Composites

Mohamed Nasr Saleh[a,1*], Hassan M. El-Dessouky[b,c,1*], Milad Saeedifar[a], Sofia Teixeira De Freitas[a], Richard J. Scaife[b], Dimitrios Zarouchas[a]

[a] Structural Integrity & Composites, Faculty of Aerospace Engineering, Delft University of Technology, Delft, 2629 HS, The Netherlands

[b] Composite Centre, AMRC with Boeing, University of Sheffield, Rotherham S60 5TZ, UK

[c] Physics Department, Faculty of Science, Mansoura University, Mansoura 35516, Egypt

[1] *Co-first author*

[*] *Corresponding authors: m.a.s.n.saleh@tudelft.nl & h.el-dessouky@sheffield.ac.uk*

Abstract

This paper investigates the effect of the fabric architecture and the z-binding yarns on the compression after multiple impacts behavior of composites. Four fiber architectures are investigated: non-crimp fabric (NCF), 2D plain weave (2D-PW), 3D orthogonal plain (ORT-PW) and twill (ORT-TW) weave. The specimens were subjected to single and multiple low-velocity impacts at different locations with the same energy level (15 J). Non-destructive techniques including ultrasonic C-scanning, X-ray CT and Digital Image Correlation (DIC) are employed to quantitatively analyze and capture the Barely Visible Impact Damage (BVID) induced in the specimens. Although the absorbed energy was approximately the same, damage was the least in 3D woven architectures. In the case of compression after impact, 3D woven composites demonstrated a progressive damage behavior with the highest residual strength (~92%) while 2D plain weave and NCF specimens showed suddenly catastrophic damage and the residual strength of ~65% and ~55% respectively.

Keywords: A. 3-Dimensional reinforcement; B. Impact behaviour; B. Damage tolerance; D. Non-destructive testing; Repeated impact

1 Introduction

Fiber-reinforced composites are widely used in automotive, oil and gas, aerospace and wind energy industries nowadays thanks to their high strength and stiffness to weight ratio compared to traditional metals. Two-dimensional (2D) composites, made of unidirectional or woven plies, are the most popular types used in industrial applications. Although they possess relatively high strength and stiffness in the in-plane direction, they are characterized by poor transverse "out-of-plane" properties especially when subjected to impact loading. It does not require high velocity impacts to induce severe internal damage into such 2D composite laminates. Thus, Low Velocity Impacts (LVI) has been a serious threat to their use in real life applications as they cause Barely-Visible Impact Damage (BVID). BVID, in fiber-reinforced composites, is one of the most critical damages in different industries, such as aerospace [1], maritime [2] and oil and gas [3], as it can go undetected while causing a significant, more than 50% [4], degradation that might lead to catastrophic failure. Generally, composite structures, such as aircrafts and composite pipes for instance, are susceptible to LVI during maintenance or ground handling. These impacts can happen because of tools dropping or support-trucks accidents, for instance. According to a report published by Boeing [1], three major causes resulted in most of the repairs for the Boeing 747 fuselage in the course of its service life. These were fatigue cracks (57.6 %), corrosion (29.4 %) and impact damage (13.0 %). Impact induced damage leads to matrix cracking, delamination, fiber matrix debonding and fiber breakage leaving only small indents on the impacted surface. To mitigate such problems, large safety margins are usually introduced in the design process of composite components and structures, which in return reduces significantly their competence with metals. With the advancement in the technical textile and weaving industries, three-dimensional (3D) woven composites have been introduced as an alternative to 2D composites whereby the out-of-plane properties are improved. Thanks to their unique characteristic of through-thickness reinforcement in resisting the delamination and transverse matrix cracking growth [5–9], 3D woven composites have been recently used in aerospace industry in as subcomponents for engines and landing gears [10,11] and potentially demonstrated for automotive applications [12].

To quantify the performance of composite materials in the out-of-plane loading, two conventional indicators are defined. The first is the impact resistance of the composite material characterized by the absorbed energy and the level of induced damage due to a specific impact energy. The second is the damage tolerance, defined as the ability to maintain the undamaged or initial strength and quantified by measuring their residual strength [11] after impact in tension (TAI), compression (CAI) and flexure (FAI). Shah et al. [11] classified the various factors affecting the impact resistance and damage tolerance of composite materials into primary and secondary ones, based on the significance of their effect. The primary factors are the fabric architecture and the resin toughness. The secondary factors include, but not limited to: environmental conditions, stacking sequence, impactor geometry and repeated impacts.

Several studies investigated the impact resistance of unidirectional (UD) [4], non-crimp fabric (NCF) [13], 2D [14,15] and 3D [8,14,15] woven composites subjected to LVI. In the case of 2D laminated composites, some researchers [16,17] tried to optimize the stacking sequence to improve the impact resistance by improving the interlaminar fracture toughness. They concluded that by changing the stacking sequence, interlaminar fracture can be suppressed or delayed by changing the load “interlaminar stresses” from tensile to compressive between the plies. For 3D woven composites [15,18], the through thickness reinforcement was found to increase the delamination resistance due to impact as well as energy absorption compared to their 2D counterparts. Besides, by changing the properties of the through-thickness yarns, the performance can be significantly improved. Damage tolerance of UD [16,19], NCF [20], 2D and 3D woven composites [14,15,19] were investigated via CAI, TAI and FAI testing. Potluri et al. [19] studied the effect of fabric architecture on the damage tolerance under CAI loading. They compared UD, 2D and 3D woven composites. They concluded that 3D woven composites demonstrated the highest residual strength, but they also observed that there is a critical damage size below which there is no significant difference in the residual strength for 3D woven composites. Hart et al. [15] compared the residual strength of 2D vs. 3D woven composites using CAI and FAI testing. Two main remarks were made. The first was that the 3D woven composites had the least reduction in strength due to the z-binding yarns suppressing delamination growth. The second was that FAI could be an attractive alternative testing approach to CAI as the reduction of strength due to impact was better captured. In other words, FAI was found to be more sensitive to delamination and damage due to impact compared to CAI. This could be attributed to the size of the impacted region compared to the specimen dimensions and the nature of the load in flexure being more dependent on the load-bearing element “fibers” in the tested composites.

With less work [1–3,21–24] focusing on the effect of repeated impacts on the residual strength of fiber-reinforced composites, most of researchers investigated only the repeated impacts occurring at the same location. Baucom et al. [24], for instance, compared the effect of repeated impacts on various fabric architectures including 2D and 3D composites. They observed that 3D woven composites absorb more energy and distribute the damage on a larger area in the form of matrix cracking and fiber-matrix debonding. While in the case of 2D composites, dominant damage mechanisms were matrix cracking, excessive delamination and fiber breakage.

From an application point of view, repeated impacts might occur to the same composite structure but at different locations, which, to the authors' knowledge, has not been thoroughly investigated in the literature. Thus, the motive for this study is to simulate multiple impacts with the same energy level at different locations for different composite architectures and study their effect on the residual strength in CAI. An extensive experimental campaign is, thus, developed to compare the single vs. multiple impact response of two 2D laminated composites, represented by NCF and 2D plain woven architectures, as well as two 3D woven composites, represented by orthogonal plain and twill architectures, as described in Section 2. Section 3 details the experimental procedure for both single and multiple impact testing, the use of NDT techniques such as ultrasonic C-scanning and X-ray computed tomography (CT) to quantify the level of induced damage and the residual strength determination using the CAI testing. Then, the discussion of the impact and CAI responses, for the four tested architectures, is reported in section 4. The comparison of the four fabric architectures is based on their response to single vs. multiple impact, the impact resistance, their damage tolerance and failure nature. Finally, section 5 provides a summary of the main concluding remarks of this study.

2 Materials and manufacturing

2.1 Materials and architectures' design

A recently developed weave-design software (EAT-3D Composites Module) for technical weaving and complex composite structures was used to design the 2D plain (2D-PW), 3D orthogonal plain (ORT-PW) and twill (ORT-TW) weaves; each of them consists of 5 warp and 5 weft layers, including the z-binding yarns in the warp. All weaves were designed with the same drafting plan to weave fabrics with the same loom setup and just change weave designs from one preform to the other. Fig. 1 demonstrates the unit-cell schematic of the four different fabrics investigated in this study. The unit-cell is defined as the smallest volume element that can represent the composite constituents, geometrical features and yield homogenized properties representative for the whole structure. The main difference between the two 3D orthogonal weaves is the z-binding yarn’s path, which directly affects the unit-cell size of the weave. In the case of the ORT-PW (Fig. 1c), the binding frequency, through the thickness, is twice the binding frequency of the ORT-TW (Fig. 1d). The effect of the unit-cell size on the impact resistance and CAI response is discussed in section 4.

A modified Dornier double-rapier FT-Dobby loom was used to produce the 2D and 3D weaves. A creel of 1100 positions was loaded with T700-12k carbon fiber bobbins to warp the loom. The creel was equipped with tension system to control the tension of warp and binder during the weaving process. To produce a balanced fabric, the densities of the warp and the weft were set to be the same: 12.66 ends/cm and 12.66 picks/cm respectively. Five layers of the 2D-PW architecture (Fig. 1b) were woven simultaneously, and 5 layers of the NCF (Fig. 1a) were used so that all produced fabrics have approximately the same areal density (~2000 GSM).

2.2 Composite panels manufacturing

A resin transfer molding (RTM) tool of 500 mm x 500 mm, manufactured by Composite Integration Ltd., was used to manufacture flat composite panels. The laminate thickness was designed to be ~2.5 mm to achieve ~50 % fiber volume fraction for all the architectures. The matrix used was Gurit T-Prime 130-1 having a mixing ratio of 100/27 by wt% of resin/hardener. The tool was preheated to 80 ˚C. The resin was degassed before injection in a degassing chamber for 30 minutes, and then placed in a pressure pot. The injection occurred at 2 bars of pressure, and -1 bar of vacuum. Upon fully wetting the preform the outlet was clamped. The pressure was left on for 15 minutes to ensure the entire mold had an even pressure and to reduce voids content in the final composite, if any. The panels were left to cure, in the RTM tool, for 1 hour at 80 ˚C.

3 Experiment and characterization

3.1 Impact testing

The testing setup to produce the BVID in the different specimens' architectures is described in this section. Three repeats from each type were used in all tests. Moreover, the reasoning behind the research approach for multiple impacts using the same energy level is discussed.

3.1.1 Single impact

Impact testing for all specimens was conducted using a drop-weight tower as per the ASTM D7136 "Standard Test Method for Measuring the Damage Resistance of a Fiber-Reinforced Polymer Matrix Composite to a Drop-Weight Impact Event" [25]. Specimens were clamped using the impact support fixture designed based on the ASTM standard to have a cut-out of 125±1 mm in the length direction and 75±1 mm in the width direction. The SI units version of the ASTM D7136 is used for all specimens (see Fig. 2). For the first set of specimens, they were all impacted in the center, with a hemi-spherical impactor with a diameter of 16 mm and a mass of 4 kg, as depicted in Fig. 2a. As the scope of this study is the LVI, the impact energy was determined based on the maximum that the weakest architecture "NCF" can accommodate without reaching the perforation threshold. Higher energies such as 25, 20 and 18 J were investigated experimentally before reaching the final decision of using 15 J as the impact energy for this study.

3.1.2 Multiple impact

The motive for this section is to simulate multiple impacts with the same energy level on the different composite architectures and study their effect on the residual strength in compression. To achieve this, a second set of specimens "three of each fabric type" were impacted twice (left and right), 25 mm apart from the first impact (see Fig. 2b) with the same impactor and the same energy. The locations of the 2nd and 3rd impacts were determined in a sense to avoid any overlap between the individual impacts as the impactor diameter was 16 mm. Moreover, they were chosen to avoid any boundary effect due to the clamping fixture. As the same impact support fixture was used, the boundary conditions for the 2nd and 3rd impacts were different from the 1st impact. Detailed analysis of the effect of the boundary conditions during impact testing can be found in [14]. This change of boundary conditions due to clamping could have an effect on the depth of dent, the stiffness of the load-displacement curves and the damage area which will be discussed further in section 4.1.3. For all the conducted impacts, either single or multiple, the impact tower was equipped with a rebound catcher (see Fig. 3b) to ensure that the impactor strikes the specimen only once.

3.2 Ultrasonic C-scanning

Before carrying out the CAI testing for the single and multiple impacted specimens, ultrasonic C-scanning was used as a Non-Destructive Technique (NDT) to evaluate the level of induced damage due to impact and to provide more information about the resistance against damage growth of the different architectures of interest in this study. The system used to scan the impacted specimens is a Midas NDT system with Zeus software. It has one transmitter and one receiver transducers with a frequency of 10 MHz, and the specimens were placed in-between. The scanning speed used was 200 mm/min.

3.3 X-ray Computed Tomography (CT)

To evaluate the level of internal damage due to impact loading, X-ray CT scans were performed for the different types of impacted specimens using a Nikon XTH-320 machine. The 225 kV source with reflective target was used with a 0.125 mm copper filter. The total volume in the field of view was $22.5\times19\times5.5$ mm^3, resulting in a resolution of ~13.2 μm. The source voltage and current were set to 220 kV and 59 μA respectively. The exposure time for each radiograph was ~1.4 seconds, with 3142 radiographs being collected over 360º. The total data acquisition time was ~1.25 hours. After scanning, the raw data was used to reconstruct the 3D volume using VGSTUDIO MAX software.

3.4 CAI testing

CAI testing for all specimens was conducted according to the ASTM D7137 "Standard Test Method for Compressive Residual Strength Properties of Damaged Polymer Matrix Composite Plates" [26]. The test set up is shown in Fig. 3d. For baseline comparison, non-impacted specimens from each architecture were tested in compression using the same test setup. For the impacted specimens as previously highlighted, there were two sets of CAI testing. The single-impacted specimens (see Fig. 3a) were directly tested in compression after the first single impact (see Fig. 3d). However, the multiple-impacted specimens were tested in compression (see Fig. 3d) after going through the process of three impacts as depicted in Fig. 3a-c. The impacted specimens were loaded in compression with a displacement-controlled crosshead of 1.25 mm/min while being supported by the CAI fixture to minimize loading eccentricities and any induced specimen's bending. The crosshead displacement and the applied force were recorded using a 500 kN load-cell MTS 810 hydraulic testing machine. Three-dimensional (3D) Digital Image Correlation (DIC) system (see Fig. 3d) was calibrated using the system's manufacturer calibration plate. Then, it was used to capture the displacement contour map during the test. The DIC system used for the full-field strain measurement consisted of two 8-bit "Point Grey" cameras with "XENOPLAN 1.4/23" lenses. Both cameras had a resolution of 5 MP. ViC-Snap 8 software was used to record the speckle pattern images with an acquisition rate of 2 frames per second (fps). Then, the acquired images by ViC-Snap 8 were processed using ViC-3D 8 software. For processing, the subset size was set to 100 x 100 pixels with a step size (distance between subsets) of 7 pixels. The observation window of approximately (120 x 70) mm^2 produced an image with dimensions of (2048 x 1194) pixels.

In addition to using the 3D DIC system during the CAI test, it was utilized before the test to measure the dent depth for all types of specimens for both the single and multiple impacted cases. On average, 15 images were captured with the Vic Snap 8 software, and then processed with the same aforementioned parameters using ViC-3D 8 software. Detailed comparison of the dent depth is discussed in section 4.1.

4 Results and discussion

4.1 Impact testing

Results from the ultrasonic C-scanning for both single and multiple-impacted specimens, DIC dent depth measurements, impact load-displacement response and the energy absorption are detailed in this section.

4.1.1 Single Impact

After the first impact, the C-scan (Fig. 4) shows a clear difference for the impact damage among the four architectures. The shape of the damaged area is one of the main differences. In the case of the NCF, where there is minimal waviness in the architecture, the damage area has a cross (0º/90º) shape. The splitting in the 0º layers is due to the longer floats compared to the 90º counterpart as previously reported in [27]. Moreover, the NCF specimens are characterized by the largest damage area. This cross shape of the damaged area almost vanishes in the case of the 2D-PW, with again a relatively large damage compared to the 3D woven counterparts. For both the ORT-PW and ORT-TW, the damaged area is smaller than the NCF and 2D-PW cases with the ORT-PW having the least damaged area. Using the 3D DIC system to calculate the dent depth suggests that the depth because of the first impact is almost the same for all architectures. This can be attributed to the fact that the energy absorption for all the architectures is almost the same as discussed later in section 4.1.3.

4.1.2 Multiple Impact

For the multiple-impacted specimens, the C-scan (Fig. 5) revealed more information about the nature of the damage occurred due to the three impacts. In the case of the NCF specimens, it is again clear that the splitting along the longitudinal direction is larger than the transverse one. In addition, the three damaged areas are interconnected. This suggests that delamination propagated in the width direction, as well, causing the NCF to suffer from the largest damaged area. For the 2D-PW case, the damage propagated more in the longitudinal direction than the transverse one. Due to the waviness of the individual plies, the damaged area did not grow as much as the NCF case. Thanks to the existence of the z-binding yarns in the 3D woven composites, the damaged area is localized and no interconnection between the three impacted regions occurred. The dent depth calculations, using the 3D DIC, revealed that the NCF specimens do not only have the largest damage area, but also the deepest dent. Detailed quantitative comparison between the single and multiple impact dent depth is discussed in the following section.

4.1.3 Single vs. multiple impact

Following the discussion in the previous sections, a detailed comparison between the single and multiple impact cases can be described based on: i) the impact load-displacement response, ii) the energy absorption and damage area calculated from the C-scans, iii) the internal damage captured by X-ray CT and iv) the dent depth measured using the DIC system.

Representative impact load-displacement curves obtained from the weight-drop impact tower for the three impacts are summarized in Fig. 6 for all the architectures. As a general remark, the effect of the clamping boundary conditions due to the clamping fixture “specimens’ holder” is clear when comparing the stiffness of the load-displacement curve of the first impact with the other consequent impacts. As the first impact occurs in the middle of the specimen, it undergoes more deflection for the same load level compared to the other two adjacent impacts. This therefore results in lower stiffness and larger deformation, regardless of the architecture of the impacted specimens. When it comes to the NCF specimens (see Fig. 6a), two important observations can be made. The first is regarding the maximum load being the least among all the other architectures. The second is regarding the maximum deformation being the largest among them. This, combined with the previous discussion about the amount of damage induced in the NCF specimens due to impact, emphasizes the inferiority of laminated (NCF) composites in sustaining the out-of-plane loading. For the other architectures, either 2D (Fig. 6b) or 3D (Fig. 6c,d) woven composites, this level of impact energy (15 J) did not cause a significant difference in their response from the load-displacement point of view.

For the sake of understanding the effect of the composite's architecture on the impact resistance, it is quite common to analyze the load-displacement response in the light of the damage-induced area and the energy absorbed by the impacted specimen. Thus, Table 1 details the level of the induced damage as a percentage of the total area of the specimen, for each architecture, calculated using MATLAB image segmenter. The trend is quite similar in the case of the single-impacted and multiple-impacted specimens. The NCF specimens experience the largest damage, followed by the 2D-PW, with the ORT-PW having the least damage. This confirms what previous studies [28–33] suggested regarding the role of the z-binding yarns in resisting delamination growth in 3D woven composites for different loading conditions. This is supported by the X-ray CT slices reported later in this section.

Figure. 7a represents a typical energy vs. time impact curve [27]. It defines the difference between the elastic and absorbed energy due to impact loading. The energy is calculated as the integration of the load-displacement curve. Moreover, Fig. 7b compares the absorbed energy for all architectures after the first impact as well as the total absorbed energy after the three impacts. NCF specimens are characterized by the highest stiffness, due to the least crimp and the straightness of the fibers, compared to the 2D and 3D woven architectures. Consequently, their energy absorption was the highest with ~14 and 42 J respectively. For 2D-PW, ORT-PW and ORT-TW, the energy absorption was almost the same with ~ 13 and 38 J respectively. Therefore, in spite of the comparable absorbed energy, the difference in the induced damage is significant, with 3D woven composites resisting the most.

Generally, LVI results in internal damage such as matrix cracking, fiber damage and fiber-matrix debonding. As discussed by Shah et al. [11], the level of damage caused by LVI depends on two primary factors including the fabric architecture and resin toughness. The resin toughness factor is outside the scope of this study. Nevertheless to further understand the role of fabric architecture and the z-binding yarns in delamination and impact resistance, cross-sectional slices from the X-ray CT reconstructed volume are analyzed. Figure 8 depicts a cross-sectional slice along the warp (0°) direction, right at the location where the impactor strikes the specimen. Although the impact energy was relatively low and caused only BVID on the surface, X-ray CT slices reveal excessive delamination at the impacted region. In the case of NCF specimens (see Fig. 8a), delamination between plies, highlighted in red, spans the full width of the field of view. Moreover, the fracture of the back side of the specimen, because of the impact, indicates fiber breakage in the bottom-most plies. For 2D-PW specimens (see Fig. 8b), delamination is a bit suppressed, compared to the NCF case, due to the waviness of the plies being 2D plain woven; but it is still guided by this waviness between the plies. In the aforementioned cases, the delamination resistance is only a function of the toughness of the matrix or the plies' waviness. On the contrary, in the case of 3D woven composites (see Fig. 8c,d) delamination is arrested by the z-binding yarns. Comparing the ORT-PW (Fig. 8c) with ORT-TW (Fig. 8d), it can be concluded that the higher the frequency of the z-binding yarn in the through thickness direction "the smaller the unit-cell size", the less the delamination propagation due to impact. Another damage mechanism can also be observed in these two cases in the form of matrix cracking in the resin-rich regions, which has been reported in [34,35] as one of the drawbacks of 3D woven composites. Matrix cracking and delamination in the case of ORT-TW are more noticeable compared to their ORT-PW counterparts (see Fig. 8c, d). They can grow longer because the distance enclosed by the z-binding yarn "L" is almost twice the distance in the ORT-PW case. However in both cases, once they reach a z-binding yarn, the damage mechanism changes to a different type, which is referred to here as binder-guided delamination. The energy required to break the reinforcing z-binding yarn is higher than the energy required for the delamination or the matrix cracking to alter its direction. Once the energy of the impact is sufficient to break the z-binding yarn, like in the case of the ORT-TW (Fig. 8d), the yarn fractures.

Besides analyzing the first and consequent impacts using the C-scanning and X-ray CT slices, dent depth measurements using DIC can be also valuable. Figure 9 compares the dent depth across the width of the specimen for the single and multiple impact cases. The measured dent depth indicates the level of plastic deformation induced in the impacted specimens. Therefore, the difference among the tested architectures can be analyzed in the light of the specimens' stiffness and accordingly the elastic vs. absorbed energies. The dent depth due to the first impact (Fig. 9a), regardless of the architecture, is very similar with a maximum value of ~0.2 mm as the impact energy is relatively low. However the dent depth, in the case of the three impacts (Fig. 9b), indicates significant dependency on the composite architecture. As a general observation, the side impacts result in a deeper dent compared to the central one. This can be attributed to the previous discussion regarding the effect of the clamping boundary conditions. As expected from the stiffness and energy absorption discussion, the NCF specimens undergo the largest deformation with the highest interaction between the adjacent impacts leading to ~1.4 mm side dent depth and ~0.8 mm central dent depth. For the other architectures, the effect is less severe leading to side dent depth of ~0.3mm.

4.2 CAI testing

4.2.1 Load-displacement response

The load-displacement curves for: baseline, single impact and multiple impact specimens are shown in Fig. 10a-c. A clear distinction, between the NCF and 2D-PW from one side and the 3D woven composites (ORT-PW and ORT-TW) from the other side, is observed when it comes to the nature of the final failure. For NCF and 2D-PW, baseline and single impact (see Fig. 10 a, b), the failure is more like a catastrophic failure with a sudden drop in the compressive load and a relatively less failure displacement (~1.5 mm). In the case of multiple impact for NCF and 2D-PW (see Fig.10 c), the failure is still catastrophic but the compressive load drops in steps, each of which corresponds to failure occurring in the vicinity of one of the three impacts. On the contrary, the ORT-PW and ORT-TW 3D woven architectures (see Fig. 10 a-c) exhibit a progressive failure response with a gradual drop in the compressive load and a larger deformation indicated by the compressive displacement (~ 3.5 to 4 mm). This directly indicates the importance of the z-binding yarns in 3D woven composites in resisting the internal damage and transforming the failure behavior from a catastrophic to a progressive one.

The comparison of the residual strength, for single-impacted and multiple-impacted specimens as function of the baseline strength, is depicted in Fig. 10d. The NCF experiences the largest reduction in the residual strength for the first and the multiple impacts (~20 % & 45 % respectively). For 2D PW, the reduction in residual strength is (~25 % & 35 %) for the single and three impacts. In the case of 3D woven composites and regardless of their unit-cell size, the strength reduction is the least. In addition, it is not much different from the single and the multiple impacts (~8 %). This observation agrees well with the conclusion drawn by Potluri et al. [19] that if the damage size is less than a critical value, there is no noticeable difference in the CAI residual strength of 3D woven composites. The damage, caused by such LVI, in 3D woven composites is very localized and contained within the impact location. The fact that the damaged regions are not interconnected reduces the effect of multiple impact on the residual strength in CAI. This highlights the damage tolerance of 3D woven composites as opposed to their 2D counterparts.

In general, fiber-reinforced composites fail in axial compression by kinking of the load-bearing tows. Kinking is a failure process [36] that occurs when the applied compressive stress exceeds a threshold level and induces plastic shear flow of the resin within and surrounding an axial tow. The fibers inside the tow rotate with the increase in the load until the tow becomes unstable and breaks a long a well-defined plane known as a kink band as shown in Fig. 11a. In the case of 2D laminated composites, clusters of kink bands grow simultaneously leading to this observed sudden failure in the load-displacement curves. Moreover due to impact loading of NCF and 2D-PW, excessive delamination growth occurs between the plies creating sub-laminates [4,11,13,19,27]. These sub-laminates then fail due to fiber micro-buckling and kink bands formation as delamination increases the unsupported length and consequently, reduces the load-carrying capacity of the individual plies. In the case of 3D woven architectures, the z-binding yarns play an important role in suppressing delamination due to impact as well as constraining the kink bands formation. Cox et al. [37] investigated the mechanics of compressive damage in 3D woven composites and reported that kink bands formation occurs first in the most severely distorted tows. These tows are normally the surface tows due to the interlacement with the z-binding yarns (see Fig. 11b). Although the surface tows fail, buckling is usually constrained by the z-binding yarn at the interlacement point. Upon increasing the compressive load, more kink bands form in other distorted tows. In other words, formation of kink bands in

3D woven composites occurs as discrete geometric and sequential flaws rather than simultaneous and sudden formation as their 2D counterparts. As a result, 3D woven composites loaded in compression fail gradually at discrete locations across the whole specimen width leading to the high deformation-to-failure.

Improving the damage resistance of composite materials, due to the z-binding yarns existence, comes at another cost, which is the ultimate compressive strength in this case. Comparing the ultimate compressive load in the case of the baseline specimens (see Table 2) clearly reflects the effect of crimp in 2D and 3D woven composites. This crimp effect has been the scope of many research studies in the literature [11,28,38–41], and it confirms the trend observed in this study. NCF with the least waviness exhibits the maximum compressive strength (see Table 2), followed by the 2D-PW, then the ORT-TW and the ORT-PW withstanding the least compressive load to failure. Although all architectures are designed to have the same fiber volume fraction in each direction (0º and 90º), the waviness of the 2D-PW leads to the knock-down in strength compared to NCF. In the case of 3D woven composites, the effect of the unit-cell size and the z-binding yarns frequency becomes very significant. The ORT-TW specimens have less crimp and more importantly less stress concentration points at the interlacement point between the z-binding yarns and the in-plane warp and weft yarns compared to the ORT-PW specimens. Thus, the ultimate compressive strength of the ORT-PW specimens is found to be the least among all the studied architectures. This suggests that a trade-off, between the required ultimate strength from one side and the progressive damage and toughness from the other side, has to be always carefully considered.

4.2.2 Failure analysis

The difference in the final failure between the single and the multiple impact cases is summarized in Fig. 12. The ASTM D7137 standard defines a three-letter code to describe the failure mode. The first letter corresponds to the failure type; the second corresponds to the failure area, and the third describes the failure location. In the case of single impact, the damage is so localized and it does not cause the specimen to break in the middle. As per the standard, this gauge failure (away from the induced damage due to impact) is still considered an acceptable failure. The designated failure code for this case is LGM where L stands for lateral failure; G is gauge/away from damage failure area, and M is the middle location. This gauge failure indicates that the tested specimen is not sensitive to the induced damage, such that it fails at a compressive stress close to the undamaged compressive strength. However, as previously noted in the case of NCF and 2D-PW, the compressive strength due to single impact was relatively less than the baseline counterparts. On the other hand, all the multiple-impacted specimens fail in the middle along the impact horizontal line. The three-letter failure code for this case is LDM; where D corresponds to at/through damage failure area. This, as per the ASTM standard, is again an acceptable failure mode, and it provides a true measurement of the residual strength of the specimens for the damage-induced state. This can be explained in the light of the Saint-Venant's principle as the notch or defect existence results in substantial changes in the stresses locally, but has a negligible effect on the stresses at distances which are large in comparison with the size of the notch or defect. This is why the stress state away from the single-impacted region is not affected, and thus the specimens fail in compression at the un-supported gauge length at the top. However in the case of the multiple impacts, this local change in stress is significant as the side impacts are close to the side-boundaries of the specimen/CAI fixture.

In order to further understand the damage progression, leading to the final failure of the CAI specimens, DIC images were analyzed. The sequence of damage occurrence among the three impacts is found to be the same for all the specimens regardless of their architecture. Thus, Fig. 13 represents one example "ORT-PW" for illustration. Due to the boundary conditions of the CAI fixture constraining the specimens' edges, the damage initiates at the side impact locations almost symmetrically. Upon load increase, the damage from the side impact grows towards the central impact. Finally, the three impacted regions are connected as the damage spans the full width of the specimen.

5 Conclusion

A systematic comparison of the impact resistance and damage tolerance of single vs. multiple impacted NCF, 2D-PW, ORT-PW and ORT-TW composites was reported. All specimens were impacted with 15 J and the damage tolerance was assessed using CAI testing. The main difference between the ORT-PW and ORT-TW 3D woven architectures is the binder frequency and the unit-cell size. It was observed that regardless of the unit-cell size, 3D woven composites are more damage and delamination resistant to the transverse impact loading compared to their 2D counterparts “NCF and 2D-PW”. In addition, the smaller the unit-cell size is, the less damage the same impact energy causes .The load-displacement response of the baseline specimens, loaded in compression, revealed the clear effect of crimp on the maximum compressive strength. NCF had the maximum strength followed by 2D-PW, then ORT-TW and the least being ORT-PW. The effect of the through-thickness binding yarns, on the buckling and damage progression in compression, was captured by the difference between the NCF and 2D-PW catastrophic failure from one side as opposed to the progressive gradual failure in the case of 3D woven composites. The reduction in CAI residual strength was minimal (~8%) in the case of 3D woven composites, followed by the 2D woven composites (~35%) and maximum in the case of NCF composites (~45%). Finally, C-scanning, X-ray CT and DIC techniques were successfully employed as NDT techniques to analyze and capture the effect of impact loading and BVID on the different composite architectures in this study, which is quite essential in real life applications so that the BVID does not go undetected.

Acknowledgments

Authors would like to acknowledge the CLSP (Composites Large Scale Project) UK Catapult partners: Advanced Manufacturing Research Centre (AMRC), National Composite Centre (NCC), Warwick Manufacturing Group (WMG) and Manufacturing Technology Centre (MTC) for supporting this research.

References

[1] Vogelesang LB, Vlot A. Development of fibre metal laminates for advanced aerospace structures. J Mater Process Technol 2000;103:1–5. doi:10.1016/S0924-0136(00)00411-8.

[2] Castellanos AG, Prabhakar P. Durability and failure mechanics of woven carbon composites under repeated impact loading in Arctic conditions. Multiscale Multidiscip Model Exp Des 2018;1:157–70. doi:10.1007/s41939-018-0024-x.

[3] Demir ̄brahim, Sayman O, Dogan A, Arikan V, Arman Y. The effects of repeated transverse impact load on the burst pressure of composite pressure vessel. Compos Part B Eng 2015;68:121–5. doi:10.1016/j.compositesb.2014.08.038.

[4] Richardson MOW, Wisheart MJ. Review of low-velocity impact properties of composite materials. Compos Part A Appl Sci Manuf 1996;27:1123–31. doi:10.1016/1359-835X(96)00074-7.

[5] Hao A, Sun B, Qiu Y, Gu B. Dynamic properties of 3-D orthogonal woven composite T-beam under transverse impact. Compos Part A Appl Sci Manuf 2008;39:1073–82. doi:10.1016/j.compositesa.2008.04.012.

[6] Ji C, Sun B, Qiu Y, Gu B. Impact damage of 3D orthogonal woven composite circular plates. Appl Compos Mater 2007;14:343–62. doi:10.1007/s10443-008-9050-x.

[7] Luo Y, Lv L, Sun B, Qiu Y, Gu B. Transverse impact behavior and energy absorption of three-dimensional orthogonal hybrid woven composites. Compos Struct 2007;81:202–9. doi:10.1016/j.compstruct.2006.08.011.

[8] Seltzer R, González C, Muñoz R, Llorca J, Blanco-Varela T. X-ray microtomography analysis of the damage micromechanisms in 3D woven composites under low-velocity impact. Compos Part A Appl Sci Manuf 2013;45:49–60. doi:10.1016/j.compositesa.2012.09.017.

[9] Gerlach R, Siviour CR, Wiegand J, Petrinic N. In-plane and through-thickness properties, failure modes, damage and delamination in 3D woven carbon fibre composites subjected to impact loading. Compos Sci Technol 2012;72:397–411. doi:10.1016/j.compscitech.2011.11.032.

[10] Mouritz AP, Bannister MK, Falzon PJ, Leong KH. Review of applications for advanced three-dimensional fibre textile composites. Compos Part A 1999;30:1445–61.

[11] Shah SZH, Karuppanan S, Megat-Yusoff PSM, Sajid Z. Impact resistance and damage tolerance of fiber reinforced composites: A Review. Compos Struct 2019;217:100–21. doi:10.1016/J.COMPSTRUCT.2019.03.021.

[12] El-Dessouky HM, Saleh MN. Chapter 4: 3D Woven Composites: From Weaving to Manufacturing. Recent Dev. F. Carbon Fibers, IntechOpen; 2018, p. 51–66. doi:10.5772/intechopen.74311.

[13] Greve L, Pickett AK. Delamination testing and modelling for composite crash simulation. Compos Sci Technol 2006;66:816–26. doi:10.1016/j.compscitech.2004.12.042.

[14] Hart KR, Chia PXL, Sheridan LE, Wetzel ED, Sottos NR, White SR. Mechanisms and characterization of impact damage in 2D and 3D woven fiber-reinforced composites. Compos Part A Appl Sci Manuf 2017;101:432–43. doi:10.1016/j.compositesa.2017.07.004.

[15] Sottos NR, Chia PXL, Hart KR, Sheridan LE, White SR, Wetzel ED. Comparison of

Compression-After-Impact and Flexure-After-Impact protocols for 2D and 3D woven fiber-reinforced composites. Compos Part A Appl Sci Manuf 2017;101:471–9. doi:10.1016/j.compositesa.2017.07.005.

[16] González E V., Maimí P, Camanho PP, Turon A, Mayugo JA. Simulation of drop-weight impact and compression after impact tests on composite laminates. Compos Struct 2012;94:3364–78. doi:10.1016/j.compstruct.2012.05.015.

[17] Jang BZ, Chen LC, Wang CZ, Lin HT, Zee RH. Impact resistance and energy absorption mechanisms in hybrid composites. Compos Sci Technol 1989;34:305–35. doi:10.1016/0266-3538(89)90002-X.

[18] Wang M, Cao M, Wang H, Siddique A, Gu B, Sun B. Drop-weight impact behaviors of 3-D angle interlock woven composites after thermal oxidative aging. Compos Struct 2017;166:239–55. doi:10.1016/j.compstruct.2017.01.046.

[19] Potluri P, Hogg P, Arshad M, Jetavat D, Jamshidi P. Influence of fibre architecture on impact damage tolerance in 3D woven composites. Appl Compos Mater 2012;19:799–812. doi:10.1007/s10443-012-9256-9.

[20] Chen F, Hodgkinson JM. Impact behaviour of composites with different fibre architecture. Proc Inst Mech Eng Part G J Aerosp Eng 2009;223:1009–17. doi:10.1243/09544100JAERO451.

[21] Huang CT, Jang BP, Kowbel W, Hsieh CY, Jang BZ. Repeated Impact Failure of Continuous Fiber Reinforced Thermoplastic and Thermoset Composites. J Compos Mater 2017;25:1171–203. doi:10.1177/002199839102500906.

[22] BIENIAŚ J, SUROWSKA B, JAKUBCZAK P. Influence of repeated impact on damage growth in fibre reinforced polymer composites. Eksploat i Niezawodn - Maint Reliab 2015;17:194–8. doi:10.17531/ein.2015.2.4.

[23] Rotem A. The Strength of Laminated Composite Materials Under Repeated Impact Loading. Compos Technol Res 1988;10:74–9.

[24] Baucom JN, Zikry MA, Rajendran AM. Low-velocity impact damage accumulation in woven S2-glass composite systems. Compos Sci Technol 2006;66:1229–38. doi:10.1016/j.compscitech.2005.11.005.

[25] ASTM D7136/D7136M-15 Standard Test Method for Measuring the Damage Resistance of a Fiber-Reinforced Polymer Matrix Composite to a Drop-Weight Impact Event 2011;i:1–16. doi:10.1520/D7136.

[26] ASTM D7137/D7137M-12 Standard Test Method for Compressive Residual Strength Properties of Damaged Polymer Matrix Composite Plates. Annu B ASTM Stand 2012;i:1–17. doi:10.1520/D7137.

[27] Mubeen A. Damage Tolerance of 3D Woven Composites with Weft Binders. The University of Manchester, 2014. doi:10.1002/ejoc.201200111.

[28] Saleh MN, Yudhanto A, Potluri P, Lubineau G, Soutis C. Characterising the loading direction sensitivity of 3D woven composites: Effect of z-binder architecture. Compos Part A Appl Sci Manuf 2016;90:577–88. doi:10.1016/j.compositesa.2016.08.028.

[29] Saleh MN, Soutis C. Recent advancements in mechanical characterisation of 3D woven

composites. Mech Adv Mater Mod Process 2017;3. doi:10.1186/s40759-017-0027-z.

[30] Saleh MN, Wang Y, Yudhanto A, Joesbury A, Potluri P, Lubineau G, et al. Investigating the Potential of Using Off-Axis 3D Woven Composites in Composite Joints' Applications. Appl Compos Mater 2016;24:377–96. doi:10.1007/s10443-016-9529-9.

[31] Ivanov DS, Lomov S V., Bogdanovich AE, Karahan M, Verpoest I. A comparative study of tensile properties of non-crimp 3D orthogonal weave and multi-layer plain weave E-glass composites. Part 2: Comprehensive experimental results. Compos Part A Appl Sci Manuf 2009;40:1144–57. doi:10.1016/j.compositesa.2009.04.032.

[32] Dai S, Cunningham PR, Marshall S, Silva C. Open hole quasi-static and fatigue characterisation of 3D woven composites. Compos Struct 2015;131:765–74. doi:10.1016/j.compstruct.2015.06.032.

[33] Midani M, Seyam A-F, Saleh MN, Pankow M. The effect of the through-thickness yarn component on the in-and out-of-plane properties of composites from 3D orthogonal woven preforms. J Text Inst 2018. doi:10.1080/00405000.2018.1481722.

[34] Saleh MN, Lubineau G, Potluri P, Withers PJ, Soutis C. Micro-mechanics based damage mechanics for 3D orthogonal woven composites: Experiment and numerical modelling. Compos Struct 2016;156:115–214. doi:10.1016/j.compstruct.2016.01.021.

[35] Lomov S V., Bogdanovich AE, Ivanov DS, Mungalov D, Karahan M, Verpoest I. A comparative study of tensile properties of non-crimp 3D orthogonal weave and multi-layer plain weave E-glass composites. Part 1: Materials, methods and principal results. Compos Part A Appl Sci Manuf 2009;40:1134–43. doi:10.1016/j.compositesa.2009.04.032.

[36] L. Tong, A.P. Mouritz MB. Chapter 5 3D Woven Composites. 3D Fibre Reinf. Polym. Compos., 2009.

[37] Cox BN, Dadkhah MS, Inman R V, Morris WL, Zupon J, International R, et al. Mechanisms of Compressive Failure in 3D Composites. Acta Metall Mater 1992;40:3285–98.

[38] Wang Y. Effect of Fabric Structures on the Mechanical Properties of 3-D Textile Composites. J Ind Text 2006;35:239–56. doi:10.1177/1528083706057595.

[39] Gerlach R, Siviour CR, Wiegand J, Petrinic N. In-plane and through-thickness properties, failure modes, damage and delamination in 3D woven carbon fibre composites subjected to impact loading. Compos Sci Technol 2012;72:397–411. doi:10.1016/j.compscitech.2011.11.032.

[40] Stig F, Hallström S. Influence of crimp on 3D-woven fibre reinforced composites. Compos Struct 2013;95:114–22. doi:10.1016/j.compstruct.2012.07.022.

[41] Saleh MN, Yudhanto A, Lubineau G, Soutis C. The effect of z-binding yarns on the electrical properties of 3D woven composites. Compos Struct 2017;182:606–16. doi:10.1016/j.compstruct.2017.09.081.

List of Figures

List of Tables

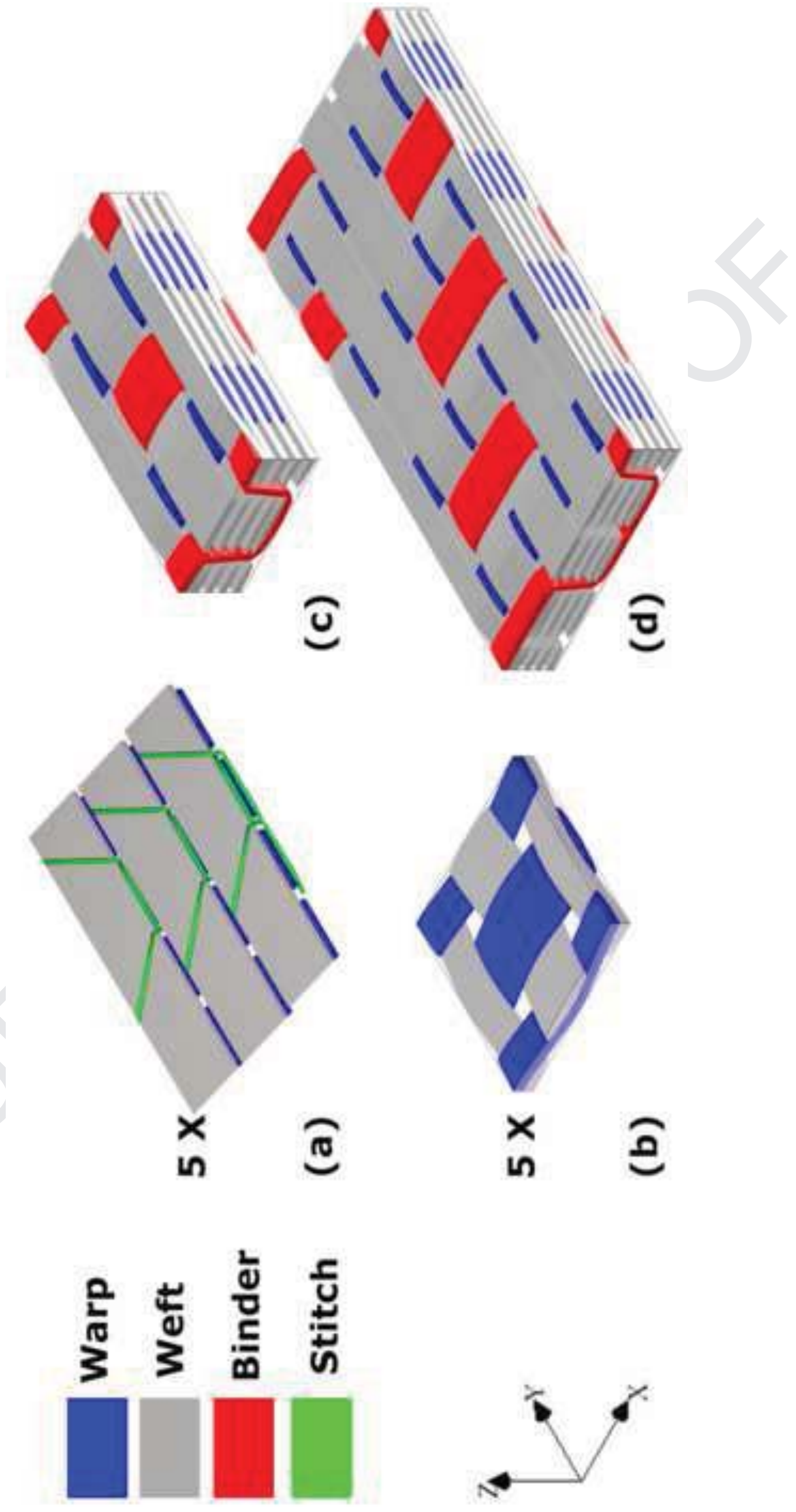
Warp
Weft
Binder
Stitch
5 X
(a)
5 X
(b)
(c)
(d)
x
y
z

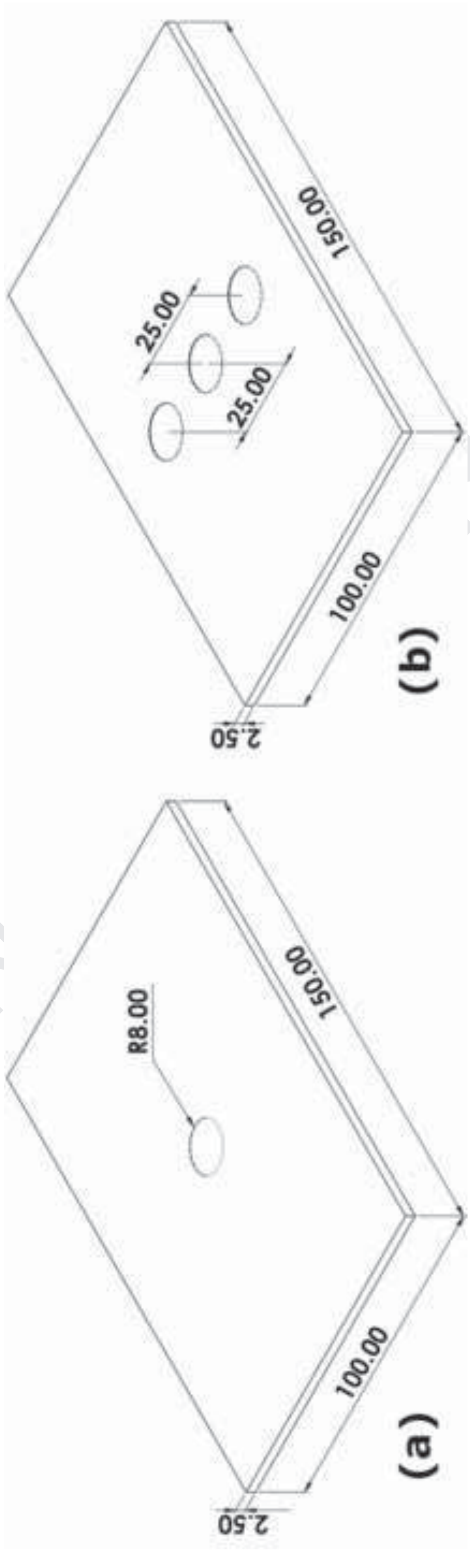
2.50
100.00
150.00
25.00
25.00
(b)
2.50
100.00
150.00
R8.00
(a)

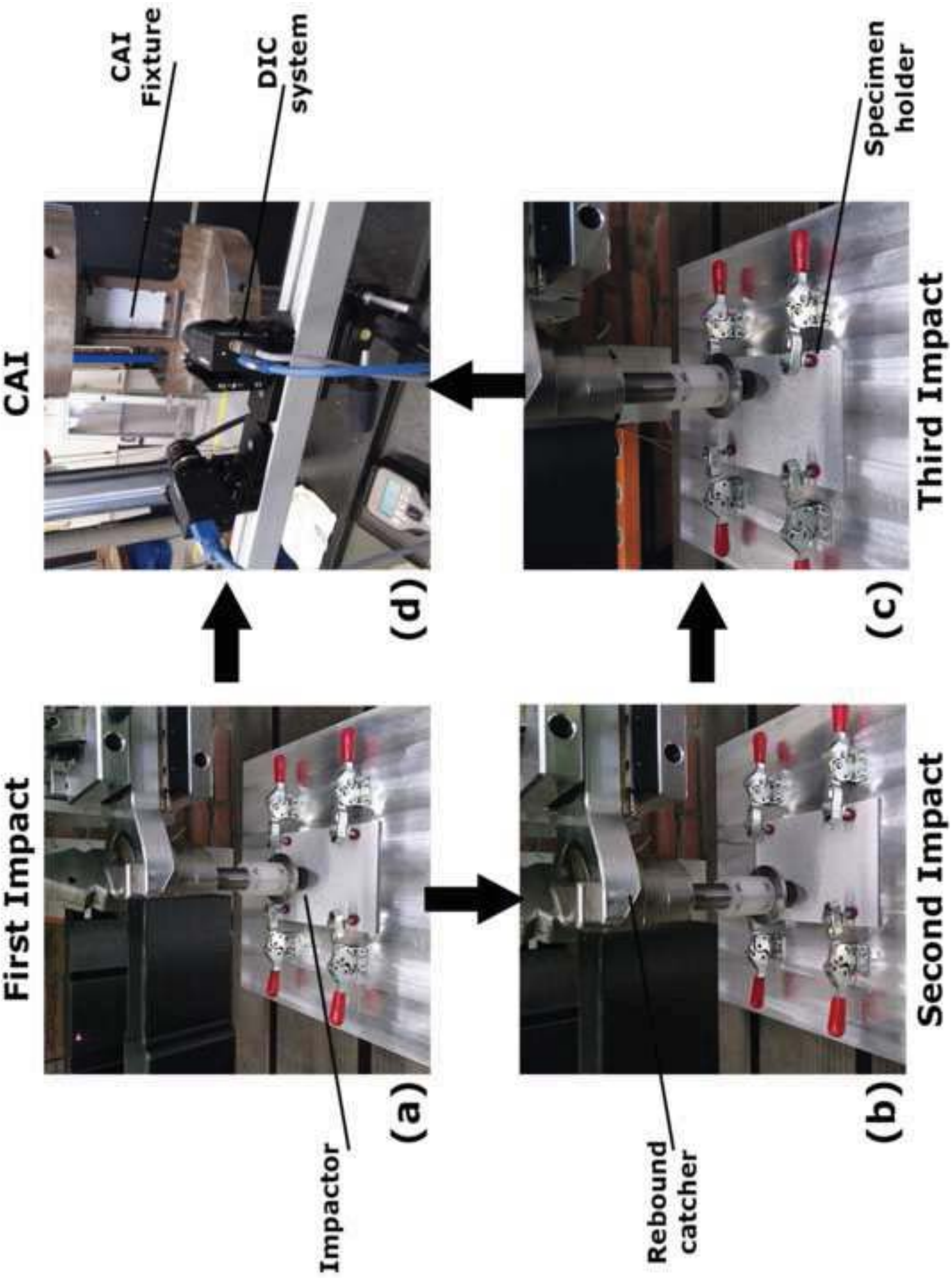
First Impact
(a)
Impactor
Second Impact
(b)
Rebound catcher
Third Impact
(c)
Specimen holder
CAI
(d)
CAI Fixture
DIC system

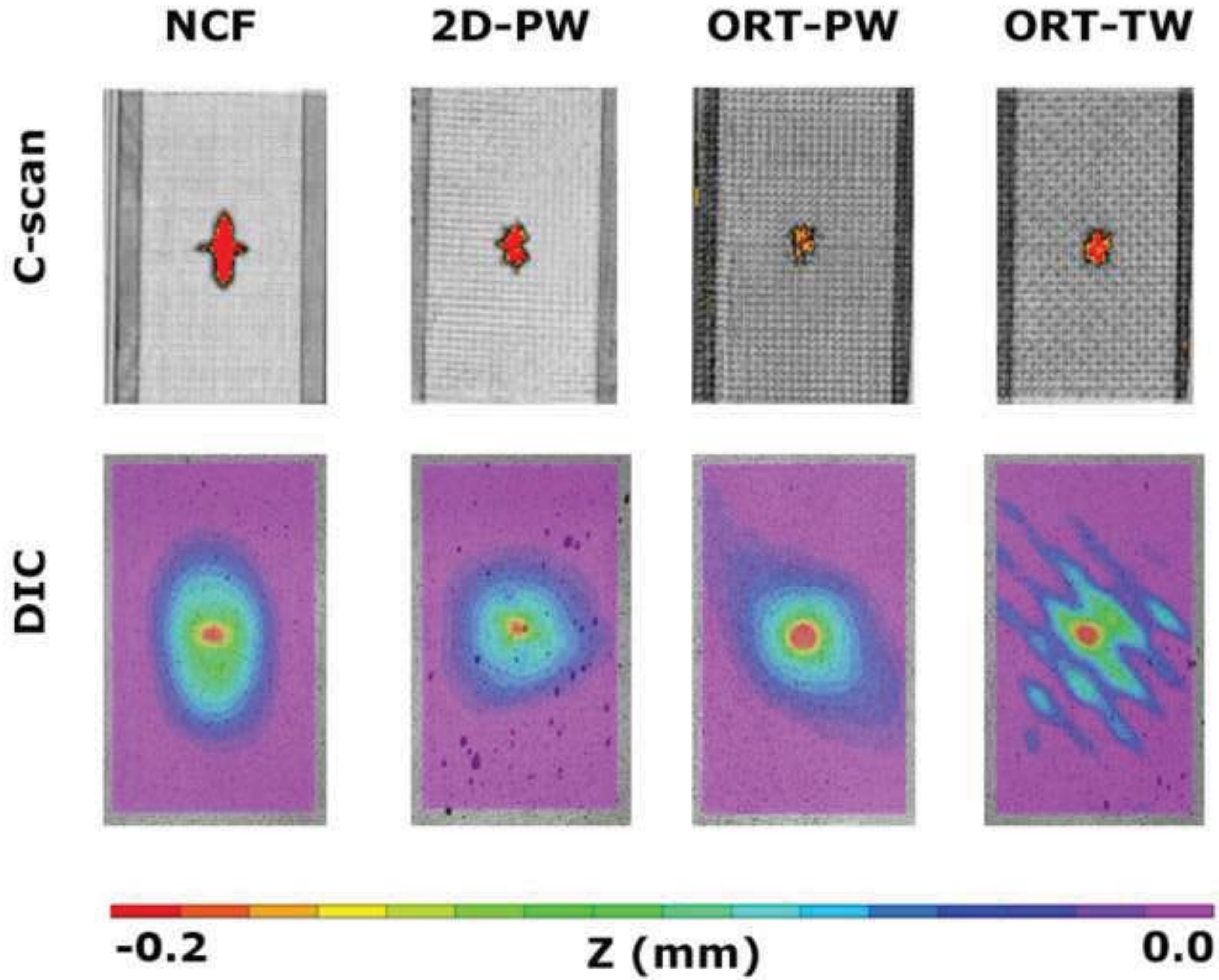
NCF
2D-PW
ORT-PW
ORT-TW
C-scan
DIC
-0.2
Z (mm)
0.0

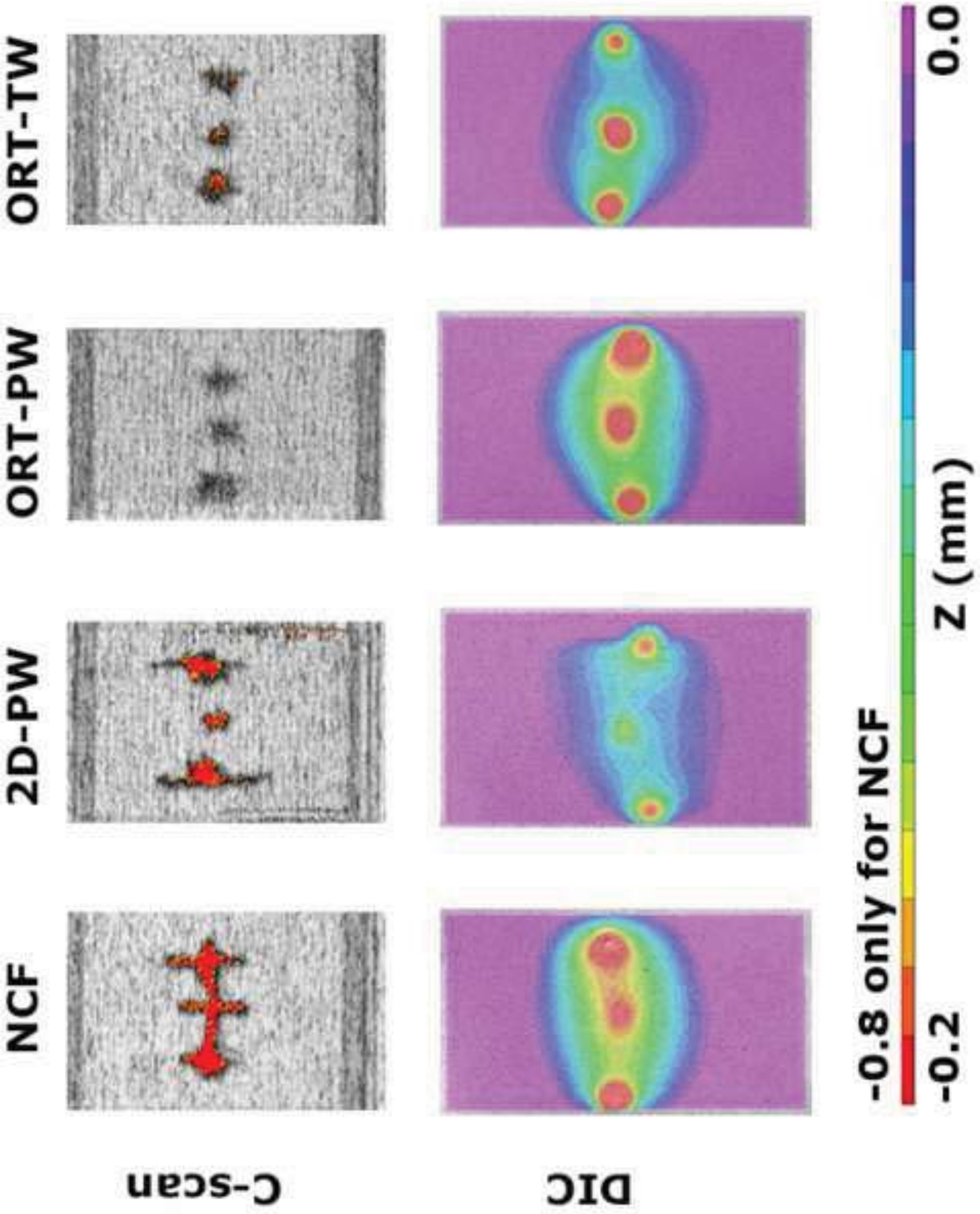
C-scan
DIC
NCF
2D-PW
ORT-PW
ORT-TW
-0.8 only for NCF
-0.2
Z (mm)
0.0

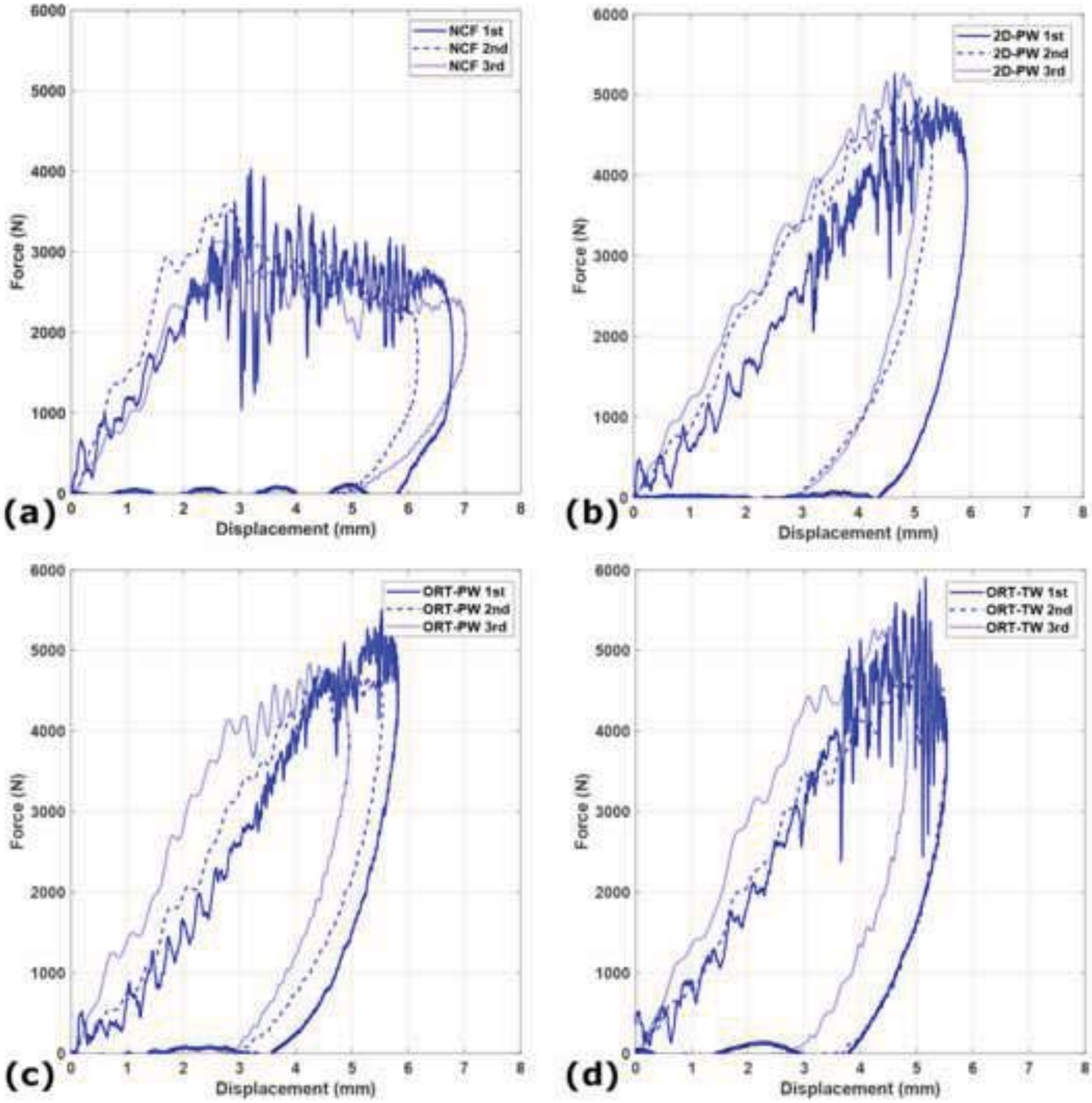
(a)
NCF 1st
NCF 2nd
NCF 3rd
Force (N)
Displacement (mm)
(b)
2D-PW 1st
2D-PW 2nd
2D-PW 3rd
Force (N)
Displacement (mm)
(c)
ORT-PW 1st
ORT-PW 2nd
ORT-PW 3rd
Force (N)
Displacement (mm)
(d)
ORT-TW 1st
ORT-TW 2nd
ORT-TW 3rd
Force (N)
Displacement (mm)
0
1000
2000
3000
4000
5000
6000
0
1
2
3
4
5
6
7
8

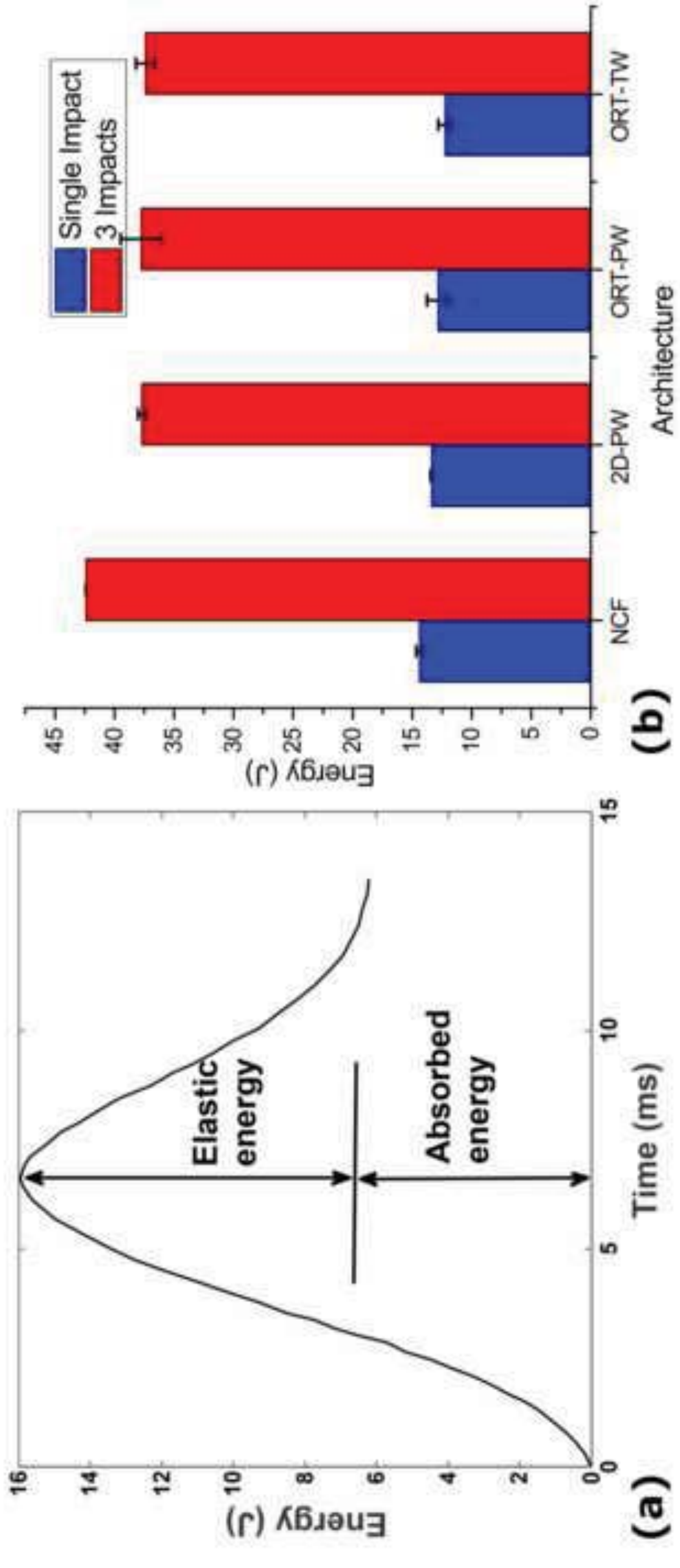
(a)
Energy (J)
0
2
4
6
8
10
12
14
16
Time (ms)
0
5
10
15
Elastic energy
Absorbed energy
(b)
Energy (J)
0
5
10
15
20
25
30
35
40
45
Architecture
NCF
2D-PW
ORT-PW
ORT-TW
Single Impact
3 Impacts

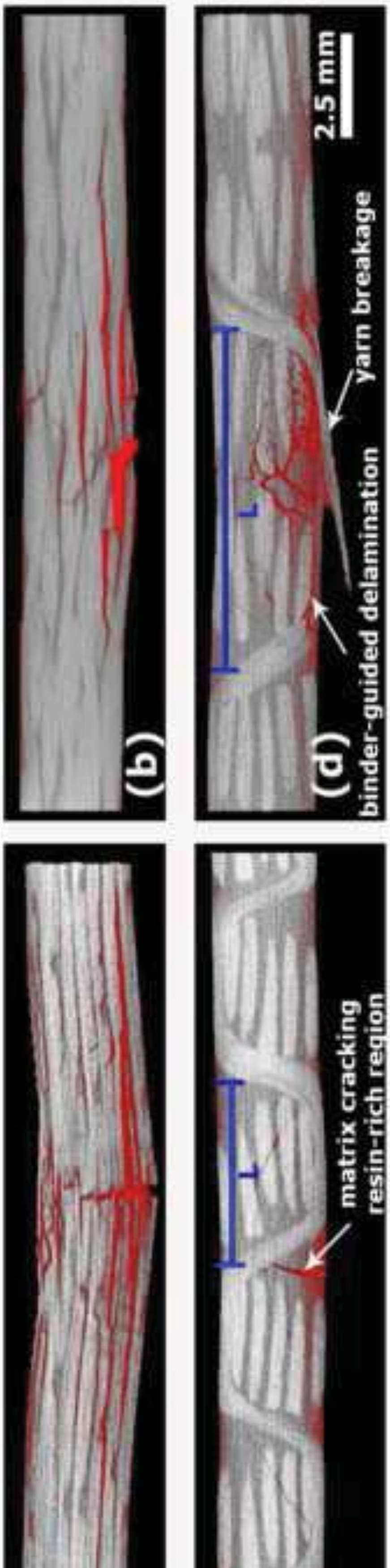
(a)
(b)
(c)
matrix cracking
resin-rich region
L
(d)
binder-guided delamination
yarn breakage
L
2.5 mm

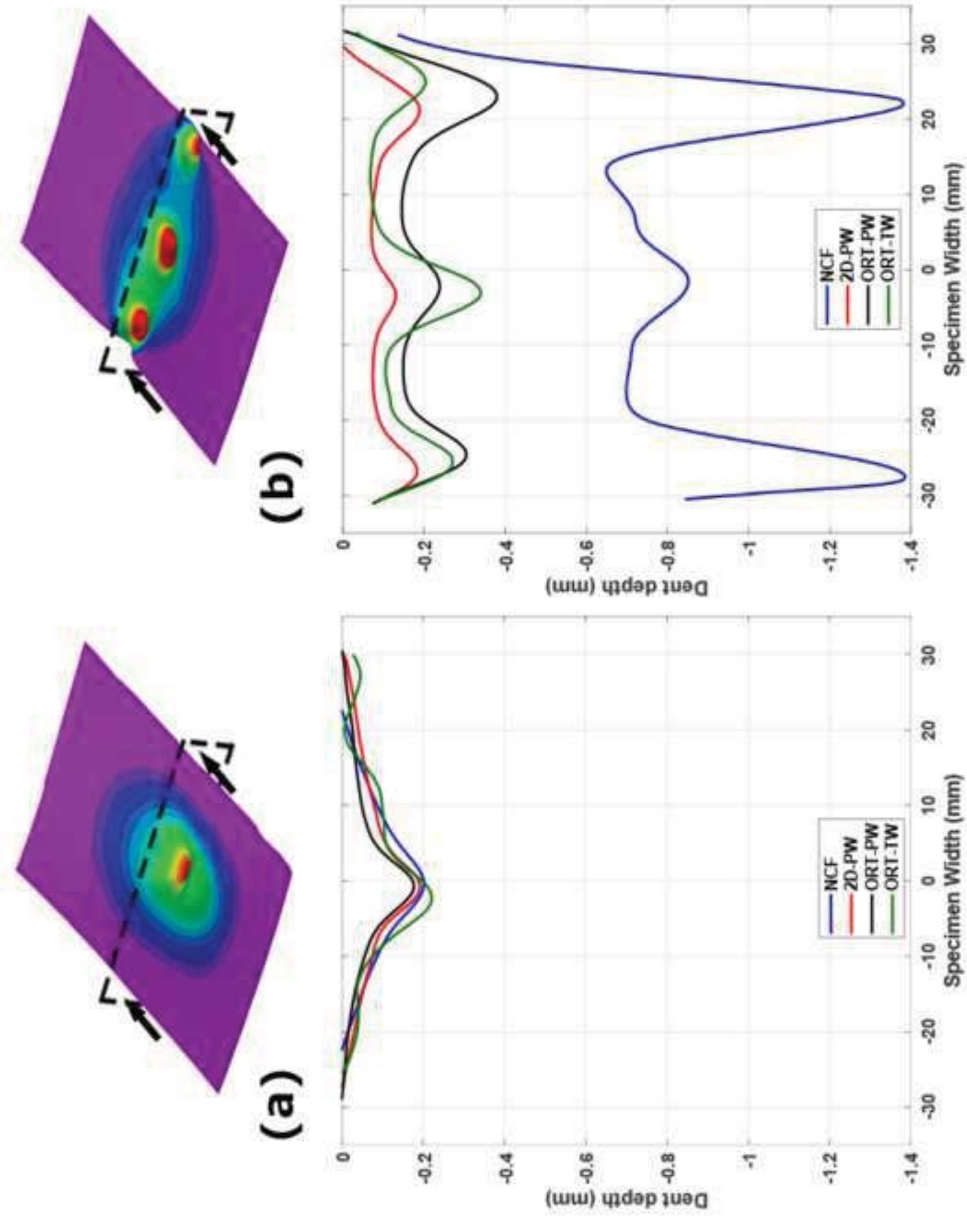
(a)
(b)
Dent depth (mm)
0
-0.2
-0.4
-0.6
-0.8
-1
-1.2
-1.4
Specimen Width (mm)
-30
-20
-10
0
10
20
30
NCF
2D-PW
ORT-PW
ORT-TW

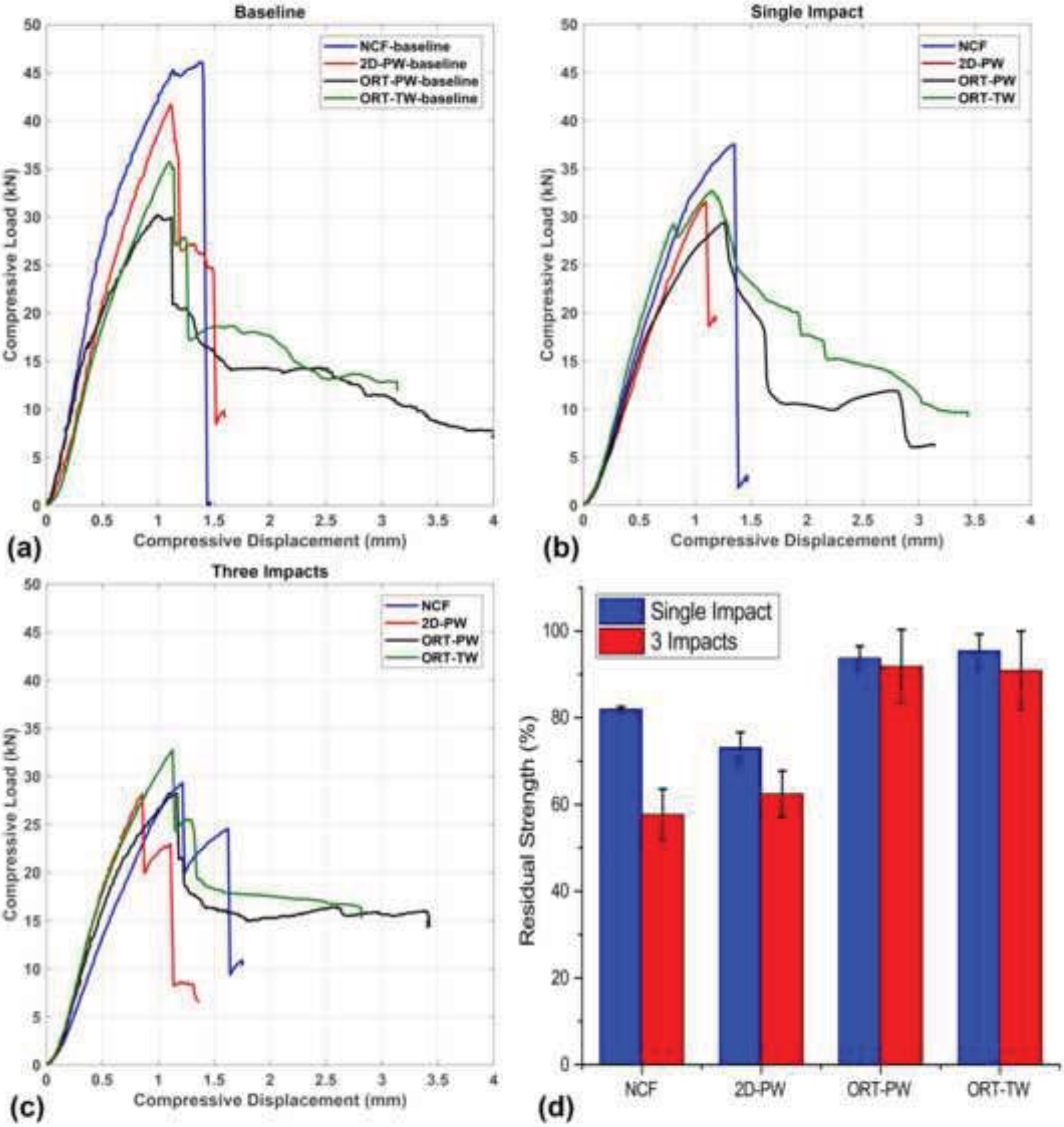
Baseline
NCF-baseline
2D-PW-baseline
ORT-PW-baseline
ORT-TW-baseline
Compressive Load (kN)
Compressive Displacement (mm)
(a)
Single Impact
NCF
2D-PW
ORT-PW
ORT-TW
Compressive Load (kN)
Compressive Displacement (mm)
(b)
Three Impacts
NCF
2D-PW
ORT-PW
ORT-TW
Compressive Load (kN)
Compressive Displacement (mm)
(c)
Single Impact
3 Impacts
Residual Strength (%)
NCF
2D-PW
ORT-PW
ORT-TW
(d)

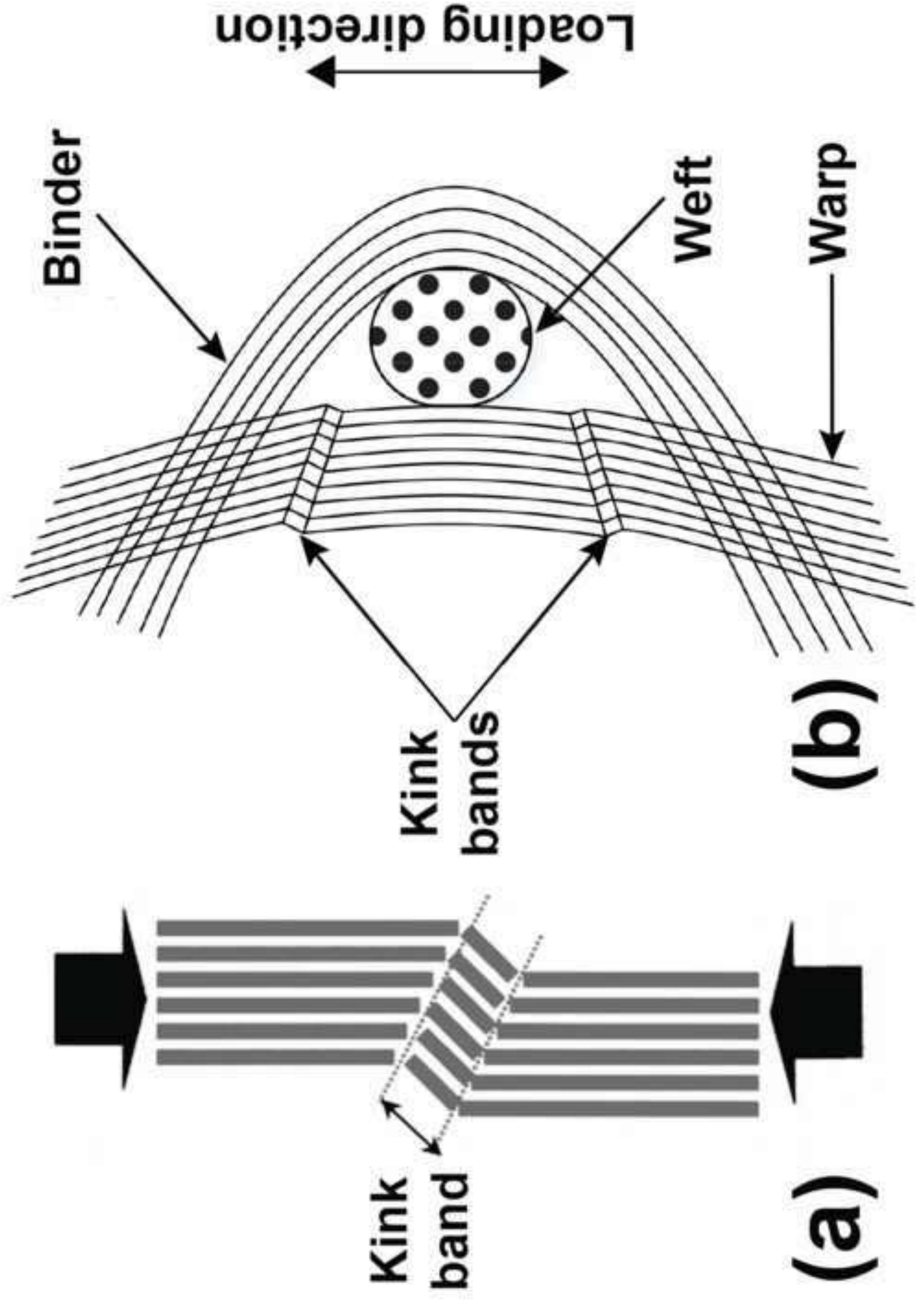
Loading direction
Binder
Weft
Warp
Kink bands
(b)
Kink band
(a)

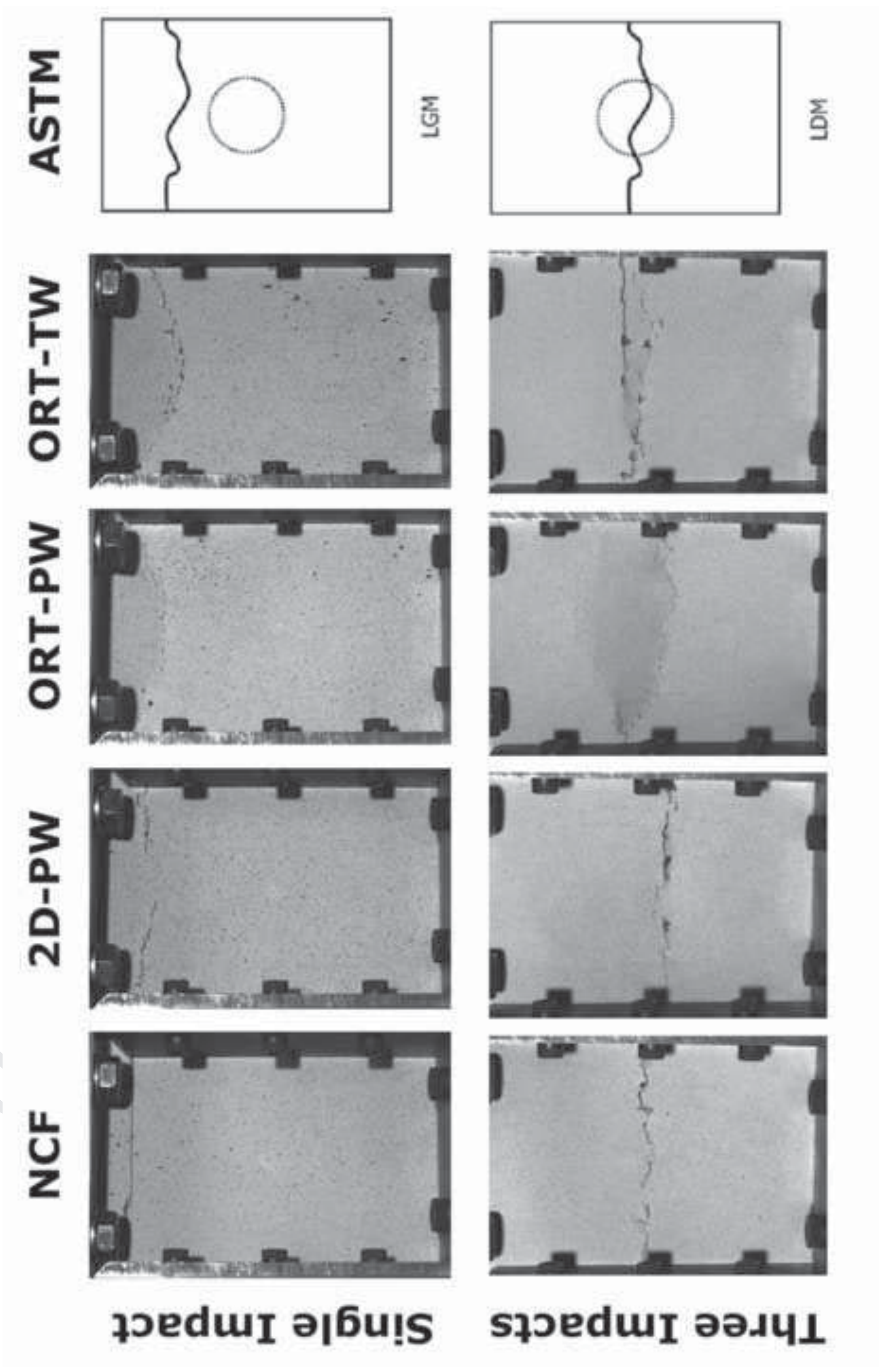
NCF
2D-PW
ORT-PW
ORT-TW
ASTM
Single Impact
Three Impacts
LGM
LDM

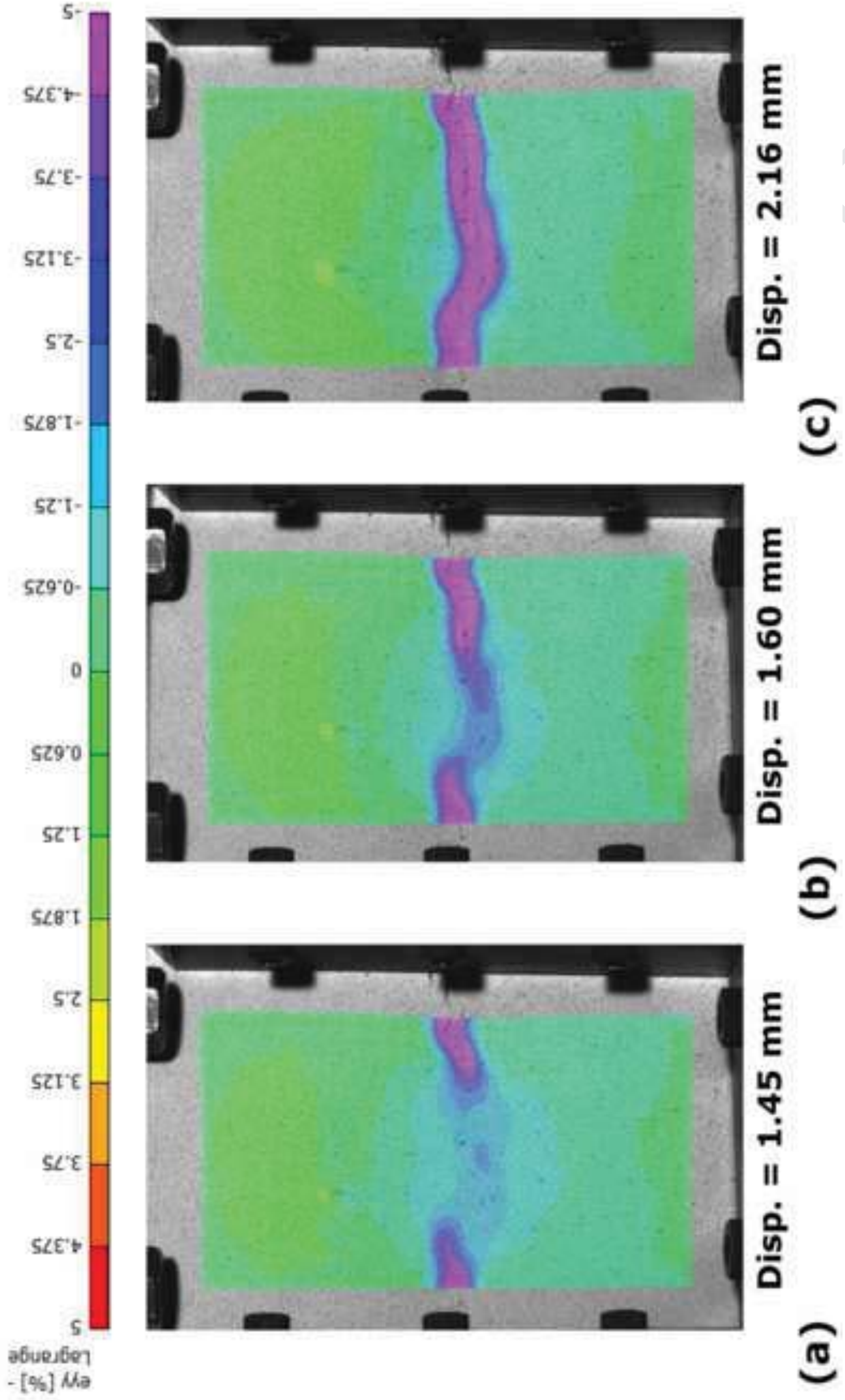
eyy [%] - Lagrange
5
4.375
3.75
3.125
2.5
1.875
1.25
0.625
0
-0.625
-1.25
-1.875
-2.5
-3.125
-3.75
-4.375
-5
(a)
Disp. = 1.45 mm
(b)
Disp. = 1.60 mm
(c)
Disp. = 2.16 mm

Table 1 Summary of the percentage of damaged area for single and multiple impacts

Architecture	Single Impact	Multiple Impacts
NCF	1.81 ± 0.29	4.01 ± 0.11
2D-PW	1.05 ± 0.12	2.35 ± 0.16
ORT-PW	0.66 ± 0.08	1.43 ± 0.27
ORT-TW	1.02 ± 0.03	1.88 ± 0.14

Table 2 Maximum compressive force (kN) for baseline, single and multiple impact cases

Architecture	Baseline	Single Impact	Multiple Impacts
NCF	46.11 ± 1.45	37.80 ± 0.27	26.59 ± 2.72
2D-PW	41.69 ± 1.85	30.49 ± 1.48	26.03 ± 2.22
ORT-PW	30.17 ± 1.69	28.29 ± 0.83	27.71 ± 2.57
ORT-TW	35.69 ± 2.30	34.06 ± 1.39	32.45 ± 3.24